Weiss, M. A., Frank, B. H., Khait, I., Pekar, A., Heiney, R., Shoelson, S. E., & Neuringer, L. J. (1990) *Biochemistry 29*, 8389–8401.
Weiss, M. A., Hua, Q. X., Frank, B. H., & Shoelson, S. E. (1991) *Biochemistry* (in press).
Wollmer, A., Fleischhauer, J., Strassburger, W., Thiele, H., Bradenburg, D., Dodson, G., & Mercola, D. (1979) *Biophys. J. 20*, 233–243.
Wollmer, A., Strassburger, W., Glatter, U., Dodson, G. G., & McRittel, W. (1981) *Hoppe-Seyler's Z. Physiol. Chem. 362*, 581–591.
Wuthrich, K. (1986) *NMR of Proteins and Nucleic Acids*, John Wiley & Sons, New York.
Wuthrich, K. (1990) *Methods Enzymol. 177*, 125–131.
Wuthrich, K., Wider, G., Wagner, G., & Braun, W. (1983) *J. Magn. Reson. 55*, 311.

ESR Spectra Reflect Local and Global Mobility in a Short Spin-Labeled Peptide throughout the α-Helix → Coil Transition†

A. P. Todd and G. L. Millhauser*
Department of Chemistry and Biochemistry, University of California, Santa Cruz, California 95064
Received August 27, 1990; Revised Manuscript Received March 9, 1991

ABSTRACT: A series of short alanine-based synthetic peptides (16 or 17 residues) have previously been shown to exhibit an anomalously high degree of α-helicity [Marqusee, S., et al. (1989) *Proc. Natl. Acad. Sci. U.S.A. 86*, 5286–5290; Marqusee, S., & Baldwin, R. L. (1987) *Proc. Natl. Acad. Sci. U.S.A. 84*, 8898–8902]. These peptides are ideal models for extracting position-dependent structural and dynamic information. Using the methanethiosulfonate nitroxide spin label (MTSSL), we labeled an analogue of the salt-bridge-stabilized "i+4" peptide, called the "i+4c", which has a specific attachment site created by replacing the central alanine with a cysteine. Circular dichroism (CD) spectra demonstrate that the i+4c-MTSSL peptide retains nearly the same helicity as the original i+4 peptide. The ESR spectra of the labeled peptide indicate no significant aggregation. ESR spectra were acquired throughout the helix–coil transition by temperature variation. From the motionally narrowed spectra, we extracted the rotational correlation times of the nitroxide label. Parallel measurements with circular dichroism enabled us to relate these parameters directly to the fractional helicity. For comparison, we followed a similar procedure with MTSSL-labeled glutathione (GS-MTSSL), a tripeptide that does not form an α-helix. Our results are interpreted in terms of a local tumbling volume, V_L, which reflects the portion of the peptide that reorients with the nitroxide label. At high fractional helicity, V_L is similar to the volume expected for a 17-residue helix. Only when the fractional helicity is lowered below 40% does V_L decrease, thereby indicating the onset of segmental motion of the peptide backbone. We analyze these results in terms of both a cooperative and a noncooperative model of the α-helix → coil transition, and we propose that the simplest cooperative view is not complete. Our experimental results and analysis show that spin label ESR is an excellent tool for rapidly extracting important structural information from nanomole quantities of peptide.

The α-helix is the most common type of secondary structure found in proteins, and the formation of α-helix from the random coil is the most well-characterized folding transition. Nevertheless, the dynamics of the α-helix → coil transition remain poorly understood. For example, it is not known whether helix formation is all-or-none (highly cooperative) or develops in a graded manner (noncooperative) in short peptide molecules. Experimental results have come almost exclusively from long-chain homopolypeptides. Thus, little is known about the transition for heterooligomers in aqueous solution, which are more appropriate models for the folding of naturally occurring proteins. Zimm–Bragg (1959) theory, along with helix/coil parameters (σ and s) from host–guest studies (Sueki et al., 1984), suggests that short peptides (<20 residues) containing helix-forming amino acids will be just on the threshold of exhibiting measurable helical structure (Shoemaker et al., 1985).

Experimentally, short helical peptides do appear to be relatively rare although there are several examples beginning with the C- and S-peptide fragments of ribonuclease A (Brown & Klee, 1971). Recently, a series of 16- and 17-residue alanine-based peptides have been synthesized (Marqusee & Baldwin, 1987; Marqusee et al., 1989) and found to have a helical content of greater than 70% at 1.0 °C. The enhanced helical stability in these peptides results partly from position-dependent effects ignored by the Zimm–Bragg theory. However, it has been proposed that the more important contribution arises from a high helix/coil equilibrium constant (s value) for alanine, which was previously underestimated in host–guest studies (Marqusee et al., 1989). Such peptides afford the exciting opportunity of studying molecular structure and dynamics in short helical segments.

The most helical of this series of synthetic peptides is the "i+4(E,K)", which is a 17-mer with positively charged lysine residues at positions 6, 11, and 16, negatively charged glutamate residues at positions 2, 7, and 12, and alanine residues at all other positions. In addition to the high helical propensity for alanine, the helical form of this peptide is stabilized by charged group interactions with the helix dipole and by salt bridge formation between lysine and glutamate residues oc-

†This work was supported by a grant from the National Science Foundation (DMB-8916946). Portions of this work were also supported by faculty research funds granted by the University of California, Santa Cruz. Acknowledgement is made to the donors of the Petroleum Research Fund, administered by the American Chemical Society, for partial support of this research.

0006-2960/91/0430-5515$02.50/0

Scheme I

curring four positions apart in the sequence. This peptide has a fractional helicity of 80% ($\Theta = 0.8$) at 1.0 °C (pH 7, low salt) and exhibits a thermal melting transition as the temperature is increased to 60 °C.

In this work, we investigate the helix–coil transition of a close analogue of the i+4(E,K) peptide that differs by the replacement of the alanine at position 9 (the central position) with a cysteine. We refer to this peptide as the i+4c to indicate the central location of the Cys. This cysteine provides an attachment site for the methanethiosulfonate spin label (MTSSL), which reacts specifically with free sulfhydryls and has the shortest linking arm of commercially available nitroxide spin labels. The sequence of the i+4c and a computer-generated structure of the MTSSL-labeled i+4c (which we term i+4c-MTSSL) are shown in Figure 1. As we will show, the resulting electron spin resonance (ESR) spectra are sensitive to peptide conformation throughout the α-helix $\rightarrow$ coil transition and provide insight into the cooperativity of helix formation in this peptide.

ESR provides a view of dynamics on a subnanosecond time scale and is sensitive to both isotropic and anisotropic motion. For singly spin-labeled peptides, there are no other interfering resonances. Spectra are quickly acquired (several minutes) from small samples (nanomole quantities) so that a range of conditions may be explored. The fidelity of results for spin-labeled analogues of short peptides require that the spin label (1) does not perturb the peptide structure and (2) is rigidly attached on the time scale of the peptide motions studied. As we will show, both of these requirements are met in this study.

ESR spectra were acquired throughout the helix–coil transition by variation of the temperature. From the motionally narrowed spectra, we extracted line-shape parameters that reflect changes in the anisotropy of the nitroxide motion and from which the rotational correlation time of the labeled peptide may be calculated. Similar spectral analysis was employed in studies of the α-helix $\rightarrow$ coil transition in spin-labeled homopolypeptides (Stone et al., 1965; Tsutsumi et al., 1978; Noji et al., 1980). We performed parallel measurements with circular dichroism (CD) that enabled us to relate these parameters directly to the fractional helicity. For comparison, we followed a similar procedure for MTSSL-labeled glutathione (GS-MTSSL). This tripeptide has a Cys in the second position and cannot form an α-helix. To interpret our results, we introduce the concept of a local tumbling volume V_L, which is essentially the volume of the peptide–label complex that reorients with the spin label. At high fractional helicity, V_L is equal to the volume expected for a 17-residue helix (with an attached spin label). As the fractional helicity is lowered below 40% ($\Theta = 0.4$), V_L decreases monotonically. We interpret this as the onset of segmental motion of the peptide backbone. We analyze these findings in terms of both a cooperative and a noncooperative model for helix–coil interconversion.

Materials and Methods

Materials. The i+4c peptide was synthesized by Susan Marqusee using the solid-phase method (Marqusee et al., 1989) and was a generous gift from the Robert L. Baldwin lab. Reduced glutathione was obtained from Sigma. Methanethiosulfonate spin label (MTSSL) was obtained from Reanal (Budapest, Hungary). 4-Hydroxy-TEMPO was obtained from Aldrich. Trifluoroacetic acid (TFA) was HPLC/Spectro grade and was obtained from Pierce. 2,2,2-Trifluoroethanol (TFE) was NMR grade (99.5+%) and was obtained from Aldrich.

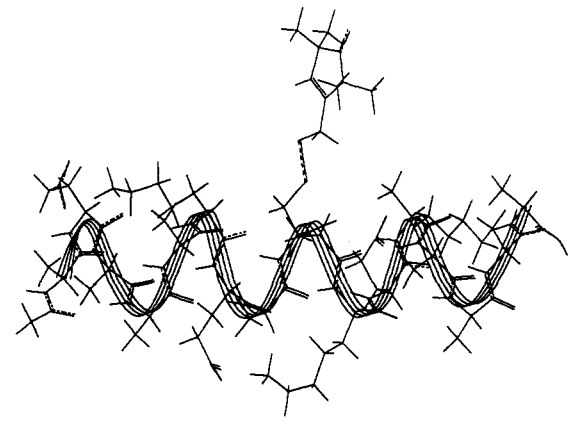

Ac-A-E-A-A-A-K-E-A-C-A-K-E-A-A-A-K-A-NH_2

FIGURE 1: i+4c-MTSSL peptide sequence and computer-generated three-dimensional structure. The energy-minimized structure (local minimum) was calculated on a personal IRIS computer (Silicon Graphics) using the program Insight II (BioSym). The nitroxide spin label (MTSSL) is the large side chain pointing up.

Peptide Spin Labeling and Purification. The unpurified i+4c peptide mixture was dissolved in 95% solvent A (water, 0.1% TFA) and 5% MTSSL stock solution (in acetonitrile) to give a slight stoichiometric excess of label. The reaction of MTSSL with i+4c to form a disulfide linkage is shown in Scheme I. The labeled 17-mer was purified by reverse-phase HPLC with a gradient of 5–45% solvent B (acetonitrile, 0.1% TFA). Reduced glutathione was spin labeled and purified by the same procedure. The molecular weight of the labeled i+4c was determined by fast atom bombardment mass spectrometry and found to be in agreement with the predicted value.

After removal of solvent under vacuum, the labeled peptide was frozen and stored at <–20 °C. Immediately prior to ESR or CD determinations, portions were thawed and redissolved in buffer (50 mM sodium phosphate, 1 mM sodium azide, pH 7), and the concentration was determined from the ESR spectrum, as described below. Following variable temperature ESR or CD, samples were checked for any degradation by HPLC.

Circular Dichroism (CD). CD spectra were acquired with an AVIV 60DS circular dichroism spectrometer calibrated with (+)-10-camphorsulfonic acid. Samples contained 50 μM peptide in the buffer described above.

Viscosities. Temperature-dependent viscosities were calculated from an empirical formula that is fit to the tabulated viscosities for pure water from 0 to 100 °C (Weast, 1973). We further determined that the 50 mM sodium phosphate buffer produced a negligible further increase in the viscosity over pure water.

Electron Spin Resonance (ESR). ESR spectra were acquired with a Bruker ESP 380 spectrometer operated in continuous wave (CW) mode with a TE_{102} rectangular cavity

and a variable temperature accessory. Samples (<5 nmol) were contained in sealed glass micropipets. To avoid line-shape distortion, the modulation amplitude was always kept to less than 1/5 of the first-derivative peak-to-peak line width. (For example, we used a modulation amplitude of 0.2 G for the high-temperature spectra and up to 0.35 G for the low-temperature spectra.) Concentrations for the labeled peptide and labeled glutathione were determined by double integration of ESR spectra followed by comparison with a standard aqueous 1.0 mM 4-hydroxy-TEMPO solution. Concentrations determined in this manner are accurate to better than 5%.

ESR Line-Shape Theory. ESR spectra are sensitive to nitroxide rotational motions over a wide range of correlation times (10^{-5} s > τ_R > 10^{-11} s). In the motional narrowing regime (τ_R < 2 ns), the three hyperfine lines are nonoverlapping with their T_2's described by

$$T_2(M)^{-1} = A + BM + CM^2 \quad (1)$$

where M is the nuclear spin quantum number of the Mth hyperfine line, $T_2(M)$ is the spin–spin relaxation time (which is inversely proportional to the homogeneous line width) of that line, and A, B, and C are the line-shape parameters. These parameters depend on the magnetic tensor principal values and the rate and anisotropy of nitroxide rotational motion. If one assumes that rotational diffusion of the nitroxide is axially symmetric, and that the diffusion tensor and the magnetic tensors are collinear, the functional form of these parameters becomes tractable. B and C alone can be used to determine rotational correlation times and general expressions for them are given below (Goldman et al., 1972):

$$B = \frac{\pi}{10}\omega_0\left[g^{(0)}D^{(0)}\left(\frac{16}{3}j_0(0) + 4j_0(\omega_0)\right) + 2g^{(2)}D^{(2)}\left(\frac{16}{3}j_2(0) + 4j_2(\omega_0)\right)\right] \quad (2)$$

$$C = \frac{4\pi^2}{5}\left[(D^{(0)})^2\left(\frac{8}{3}j_0(0) - j_0(\omega_a) - \frac{1}{3}j_0(\omega_0)\right) + 2(D^{(2)})^2\left(\frac{8}{3}j_2(0) - j_2(\omega_a) - \frac{1}{3}j_2(\omega_0)\right)\right]$$

The spectral densities are

$$j_m(\omega) = \frac{\tau(m)}{1 + \tau(m)^2\omega^2}$$

where $\tau(0) = 1/(6R_\perp)$ and $\tau(2) = 1/(2R_\perp + 4R_\parallel)$ and the spherical tensor components are

$$g^{(0)} = (1/\sqrt{6})[2g_{zz} - (g_{xx} + g_{yy})]; \; g^{(2)} = (1/2)(g_{xx} - g_{yy})$$

$$D^{(0)} = (1/2\sqrt{6})[2A_{zz} - (A_{xx} + A_{yy})]; \; D^{(2)} = (1/4)(A_{xx} - A_{yy})$$

The other symbols have their usual meanings: g_{xx}, g_{yy}, g_{zz}, A_{xx}, A_{yy}, and A_{zz} are the magnetic tensor principal components; $R_\parallel$ and $R_\perp$ are the rotational diffusion coefficients about the unique and nonunique diffusion axes; a_N is the isotropic hyperfine coupling constant to the nitrogen; γ_e is the electron gyromagnetic ratio, $\omega_a = (1/2)a_N|\gamma_e|$, and ω_0 is the electron Larmor frequency. The rotational correlation time is defined with the relation $\tau_R^{-1} = 6(R_\parallel R_\perp)^{1/2}$, and for convenience we further define $\tau_\parallel = (6R_\parallel)^{-1}$ and $\tau_\perp = (6R_\perp)^{-1}$. If isotropic motion is assumed, $R_\parallel = R_\perp$ and $\tau(0) = \tau(2) = \tau_R$ is the isotropic rotational correlation time. For a careful discussion of the quantities that describe rotational diffusion see the recent review by Beth and Robinson (1989).

In the motional regime spanned in this study (0.04–1.0 ns), the spectral densities reduce to $j_m(0) = \tau(m)$, $j_m(\omega_a) = \tau(m)$, and $j_m(\omega_0) = 0$. With this simplification the ratio $|C/B|$ becomes independent of τ_R but does depend upon the rotational anisotropy $N \equiv R_\parallel/R_\perp = \tau_\perp/\tau_\parallel$. To evaluate both τ_R and N, accurate values of the magnetic tensor components are required. The values for g_{xx}, g_{yy}, and g_{zz} have been determined for a similar nitroxide to be 2.0086, 2.0066, and 2.0032, respectively (Capiomont et al., 1974), and we use these values in our analysis. An accurate determination of the A tensor in H_2O is not available, so we estimate the principle values as follows. A_{zz} can be measured directly from frozen solutions and has been determined to be 35.7 G. Likewise, a_N can be determined from fast motional spectra and is 16.07 G (Windle, 1981). If we assume $A_{xx} \approx A_{yy}$ and we use the identity $a_N = 1/3(A_{xx} + A_{yy} + A_{zz})$ the we find $A_{xx} \approx 6.23$ G.

In order to extract motional information, one must compare the analytical expressions in eq 2 with the experimental values of B and C derived from the spectral line widths. B and C are conveniently obtained directly from the inhomogeneous first-derivative peak-to-peak line widths and line heights of continuous wave (cw) spectra if appropriate corrections are made. Expressions for B and C in terms of these parameters are

$$B = \frac{\sqrt{3}}{4}\Delta H(0)\left\{\sqrt{\frac{V(0)}{V(+1)}} - \sqrt{\frac{V(0)}{V(-1)}}\right\} \quad (3)$$

$$C = \frac{\sqrt{3}}{4}\Delta H(0)\left\{\sqrt{\frac{V(0)}{V(+1)}} + \sqrt{\frac{V(0)}{V(-1)}} - 2\right\}$$

where $\Delta H(0)$ is the peak-to-peak width of the center (M = 0) line and $V(M)$ is the peak-to-peak height of the Mth line. We could simply use the widths of the three hyperfine lines ($\Delta H(M)$; $M = -1, 0, +1$) to determine B and C; however, it has been shown that eq 3 provides a much more error-free estimate of these values (Hwang et al., 1975). Because we have defined B and C in terms of eq 1, these expressions differ by a factor $\sqrt{3}/2$ from those given in Bales (1989).

Both B and C, as determined from eq 3, still contain some systematic inaccuracies (of order <10%) due to Gaussian inhomogeneous broadening. A procedure developed by Bales (1989) corrects for this. To apply this correction, the value of the inhomogeneous line width is needed. In the MTSSL spin label, inhomogeneous broadening arises almost exclusively from weak hyperfine interactions due to the nitroxide protons. The isotropic hyperfine coupling constants have been measured for a similar label to be 0.20 G from the 12 methyl protons and approximately 0.51 G from the ring proton (Hyde & Subczynski, 1984). These interactions give rise to a total Gaussian inhomogeneous broadening of 0.9 G (Bales, 1989), and this value only changes by a few percent as a function of temperature.

Finally, from B and C, the rotational correlation times are determined from eq 2. The methods outlined above are well-established and have been used in a number of important studies [for a review see Marsh (1989)]. Nevertheless, we felt that the technique should be tested to determine any inaccuracies. To carry this out, we simulated inhomogeneously broadened spectra over a range of correlation times from 0.1 to 1.8 ns. We determined B and C from eq 3 and applied Bales corrections to remove the effects of inhomogeneous broadening. From the corrected values for B and C, we calculated the rotational correlation times and compared these quantities to the input correlation times. In all cases we found that our

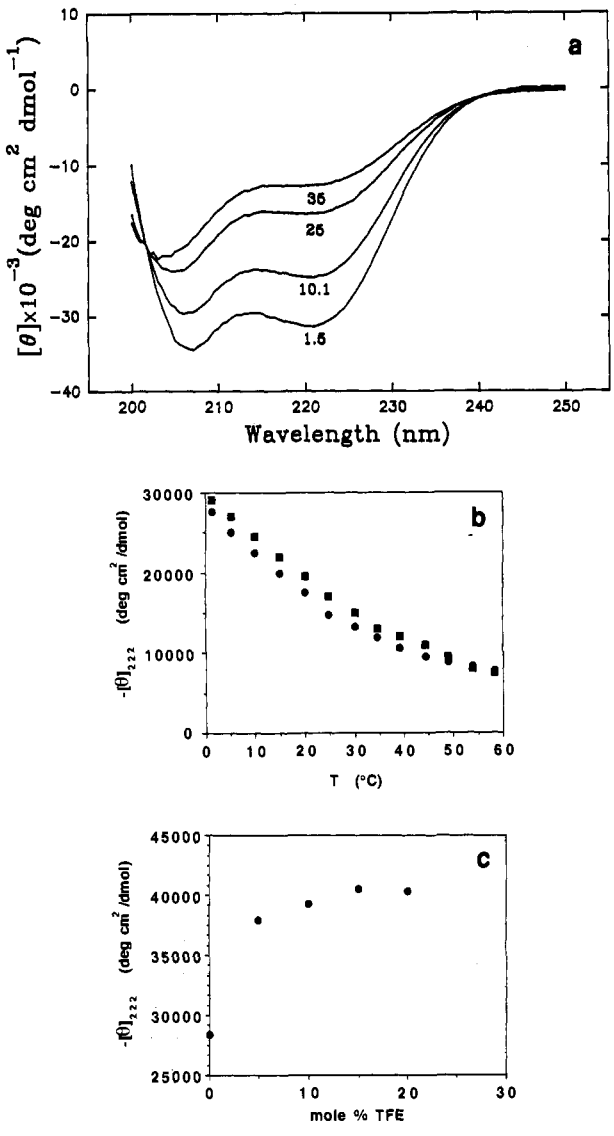

FIGURE 2: (a) CD spectra of the spin-labeled i+4c-MTSSL peptide (50 μM) in 0.05 M phosphate buffer (pH 7.0) at four temperatures (°C). (b) Thermal unfolding profile for helical peptides measured by $-[\theta]_{222}$, the mean residue ellipticity at 222 nm. Circles: spin-labeled i+4c. Squares: i+4 [from Marqusee and Baldwin (1987)]. (c) Dependence of helicity of the spin-labeled i+4c peptide (phosphate buffer, pH 7, at 1.0 °C) on TFE concentration.

calculated results were systematically greater than the input values by 4% to 6%. This systematic error is quite tolerable given that there is also a systematic error in the hyperfine tensor values of several percent. Thus, a very conservative estimate of the systematic error in our experimentally determined correlation times is 10%, and this error is uniform over the range of temperatures studied.

Results

Helix Formation Is High in Spin-Labeled i+4c. In Figure 1 is a diagram of the i+4c-MTSSL peptide as calculated using the Insight and Discover software (from BioSym) running on a Silicon Graphics Iris computer. The energy of the helix, but not the nitroxide side-chain, has been minimized in vacuum. The helix backbone is highlighted with a ribbon and two of the three $Lys^+\cdots Glu^-$ salt bridges are visible. The nitroxide spin label is visible above the backbone and provides a perspective on the size of the MTSSL side-chain relative to the size of the total peptide.

Helix formation of i+4c-MTSSL was monitored by CD and the low-temperature spectra exhibit a double minimum

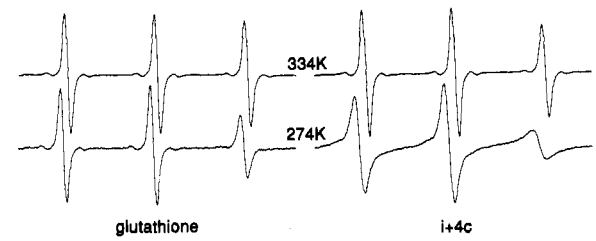

FIGURE 3: ESR spectra of the spin-labeled peptidies i+4c-MTSSL and GS-MTSSL in 0.05 M phosphate buffer (pH 7.0) at two different temperatures.

characteristic of an α-helix (Figure 2a). Helical content was quantified by the mean residue ellipticity at 222 nm ($-[\theta]_{222}$). All CD spectra were acquired at a concentration of 50 μM peptide, which is within the range where $-[\theta]_{222}$ is independent of concentration for the i+4 peptide (Marqusee & Baldwin, 1987). ESR spectra for the labeled i+4c peptide at 1.0 °C indicate no aggregation at concentrations as high as 500 μM (see below).

Helix formation in labeled i+4c exhibits a strong temperature dependence with increasing helicity at low temperature, as can be seen in Figure 2a,b. This is consistent with the helix–coil transition behavior observed for other peptides, including the i+4 peptide (Figure 2b). The mean residue ellipticity of 28 400 cm^2 deg/dmol observed at 1.5 °C for the i+4c-MTSSL peptide corresponds quite closely to the value of 29 000 cm^2 deg/dmol at 1.0 °C for the i+4 peptide (Marqusee & Baldwin, 1987). Futhermore, Figure 2a shows that there is an isodichroic point at 202 nm, indicating a superposition of two CD states, as was also observed for the i+4 peptide. These results demonstrate that the substitution of cysteine-MTSSL for alanine does not significantly perturb the helix–coil equilibrium in this peptide.

Helix formation is promoted by the addition of TFE (Nelson & Kallenbach, 1986). A titration curve of helicity vs TFE concentration is shown in Figure 2c. $-[\theta]_{222}$ reaches a maximum of about 40 500 cm^2 deg/dmol at 15 mol % TFE, and this is usually assigned to a fractional helicity of 1. However, we also performed control studies with labeled and unlabeled glutathione and found that the disulfide-linked nitroxide side chain contributed a CD signal of 1100 cm^2 deg/dmol at 222 nm in TFE (and no signal in the absence of TFE). Therefore, we estimate that $-[\theta]_{222}$ is 39 400 cm^2 deg/dmol for the 100% helical peptide and that the i+4c-MTSSL has a fractional helicity of 72% ($\Theta = 0.72$) in aqueous solution at 1.5 °C. This compares favorably with the i+4 peptide, which exhibits a fractional helicity of 80% at 1.5 °C.

Peptide Geometry Changes with Temperature and Fractional Helicity. ESR spectral line shapes are sensitive to the rotational motion of the nitroxide. In the motional narrowing regime ($\tau_R < 2 \times 10^{-9}$ s), information about the rate and anisotropy of motion of the nitroxide may be extracted from the spectra from height and width measurements of the three first-derivative hyperfine peaks (see ESR line-shape theory). As is shown in Figure 3, the spectral lines broaden at low temperatures. Likewise, there is an inequality in the height of the three lines for both of the peptides, i+4c-MTSSL and GS-MTSSL, which is increasingly pronounced at low temperature. This inequality is a qualitative index of the rate of rotational diffusion of the nitroxide and is greater with slower motion. In this case it reflects, in part, the expected slowing of rotational diffusion with lowered temperature. The spectra for the i+4c-MTSSL peptide exhibit a greater inequality in line height at all temperatures, reflecting the larger size of this peptide compared to GS-MTSSL (17 vs 3 residues). As we

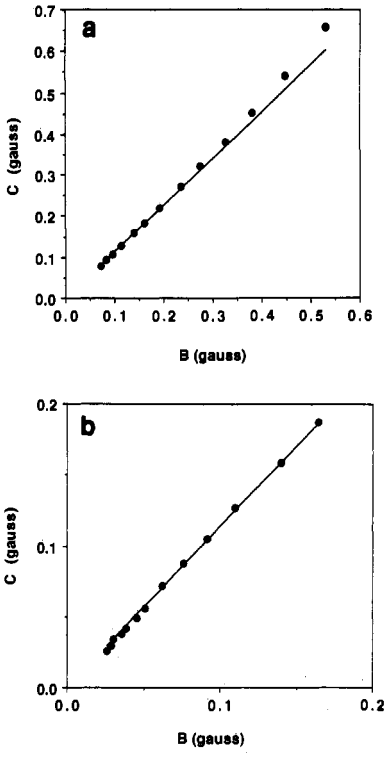

FIGURE 4: Line-shape parameters C vs $|B|$ for (a) i+4c-MTSSL and (b) GS-MTSSL. A constant slope reveals a constant motional anisotropy (N; see Results).

show below, more subtle spectral differences between the two peptides are quantified by the line-width parameters B and C that indicate changes in structure of the two peptides with temperature. None of the spectra exhibit the symmetric line broadening characteristic of Heisenberg spin exchange, which appears to rule out any observable aggregation of peptides. Aggregation would also increase τ_R and change the relative heights of the hyperfine peaks. However, spectra for two concentrations (250 and 500 μM) of the labeled i+4c at 1.0 °C were found to be exactly superimposable (data not shown).

The ratio of $|C/B|$ is independent of τ_R, in the motional regime studied here, and reflects the anisotropy of tumbling ($N \equiv R_\parallel/R_\perp = \tau_\perp/\tau_\parallel$). Because neither the elements of the magnetic tensors nor the orientation of these tensors with respect to the rotational diffusion tensors is accurately known (which was discussed above), we cannot unambiguously interpret the value of this ratio. However, changes in $|C/B|$ must reflect changes in tumbling anisotropy, and this is most easily examined in a plot of C vs $|B|$, as in Figure 4. The linear regression fit demonstrates that C vs $|B|$ is approximately linear throughout for spin-labeled glutathione, suggesting that its rotational anisotropy is approximately constant and, probably, isotropic at all temperatures. However, C vs $|B|$ for spin-labeled i+4c exhibits a deviation from linearity at low temperatures (large B and C), suggesting a small change in anisotropy of the nitroxide rotational motion. The linear regression fit from the high-temperature region has the same slope (1.12) as that found for GS-MTSSL to within 1%. (Preliminary analysis of $C/|B|$ at low temperatures suggests anisotropic motion with $N \approx 2$ about the nitroxide y axis; however, further refinement of the hyperfine tensor values is required to assure this assignment.) These observations are consistent with a change in peptide shape as a function of fractional helicity, as we discuss below.

From the parameters B and C, one can accurately calculate the rotational correlation time (τ_R) of the nitroxide. Because

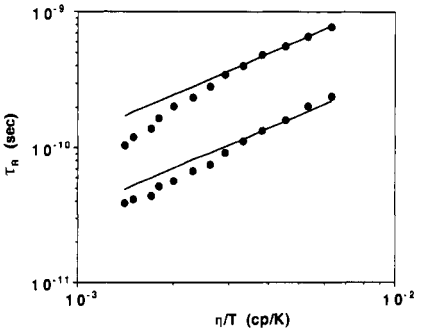

FIGURE 5: Dependence of rotational correlation time (τ_R) for spin-labeled i+4c (filled circles on upper curve) and glutathione (filled circles on lower curve) on viscosity over temperature (η/T). The solid lines are respective fits to the Stokes–Einstein relation in eq 4 (see Results).

the apparent changes in tumbling anisotropy are small for the spin labeled i+4c, we can approximate the rotational motion as isotropic and determine τ_R values from B. These results can be interpreted in terms of the Stokes–Einstein (SE) relationship for rotational motion

$$\tau_R = V\eta/kT \qquad (4)$$

where k is Boltzmann's constant, T is the absolute temperature, η is the solvent viscosity, and V is the volume of the tumbling molecule. A molecule with V = constant gives a linear relationship between τ_R and η/T, and this type of behavior has been observed in ESR studies of nitroxide spin probes (Hwang et al., 1975). In Figure 5 we show a logarithmic plot of τ_R vs η/T for both i+4c-MTSSL and GS-MTSSL. There is a small amount of random scatter, and we verified with multiple experiments that the standard deviation of the random error in our experiments is less than ±3%. At all temperatures it is clear that i+4c-MTSSL reorients much more slowly than GS-MTSSL, as expected, based on the difference in the molecular weights. The correlation time τ_R can be estimated for hydrated (approximately) spherical molecules from a semiempirical relationship derived from simple thermodynamics of hydration arguments (Cantor & Schimmel, 1980). For spin-labeled i+4c and spin-labeled glutathione, the calculated correlation times are 1.3 and 0.35 ns, respectively, at 1.0 °C. These values are reasonably close to our experimental values of 0.77 and 0.25 ns at 1.0 °C. The results for i+4c-MTSSL is also reasonable when compared to NMR studies of a 20-mer of poly(γ-benzyl-L-glutamate), which was found to have a rotational correlation time of 1.0 ns (Mirau & Bovey, 1986).

We now turn to the actual shape of the τ_R vs η/T curves. The linear regression fits shown are to the function in eq 4, which is a linear polynomial with no zeroth-order additive constant (i.e., a function of the form $y = mx$ and *not* of the form $y = mx+b$). Thus, the slopes of the fits, on this logarithmic plot, must be unity. GS-MTSSL is fit over the entire range of η/T, and i+4c-MTSSL is fit only at low temperatures; and the resulting curve is extrapolated to high temperatures. In contrast to many simple nitroxides, GS-MTSSL does not appear to follow SE behavior through most of the temperature range. The high temperature regime, however, does appear to have a slope of unity. The behavior for i+4c-MTSSL departs even more dramatically from ideal SE behavior. The low-temperature data clearly follows SE behavior up to almost room temperature. At higher temperatures the non-SE character becomes increasingly pronounced. Interestingly, the temperature regime where Stokes–Einstein behavior breaks down is the same regime that shows a change in slope of the C vs B plot. We point out that non-SE behavior

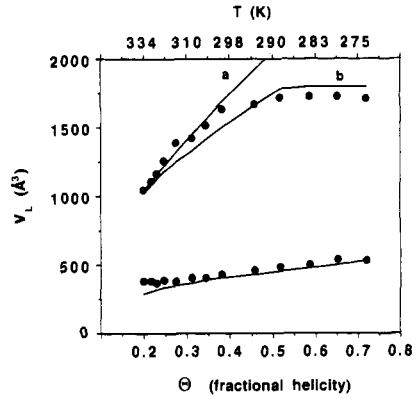

FIGURE 6: Local tumbling volume ($V_L = \tau_R kT/\eta$) as a function of fractional helicity (Θ) for spin-labeled i+4c (filled circles on upper curve). Corresponding temperatures are shown along the top axis. Spin-labeled gluathione (filled circles on lower curve) is shown as a reference at each temperature although this peptide has no helicity. Data for the i+4c-MTSSL were modeled in terms of a cooperative transition (solid line a) and a noncooperative transition (solid line b) (see Discussion). GS-MTSSL data empirically followed the function $V_L(T) = V_L(274) \times (274/T)^3$ (solid line).

has also been observed in some small nitroxides, however, the data in those experiments could be fit to an equation similar to eq 4 with an additive constant (Zager & Freed, 1982). Those results were successfully explained in terms of an approximate fluctuating torque model that gives rise to non-Debye spectral density functions. We feel that such an approach would not be successful here because a linear function with an additive constant does not provide a good fit to the data for either of our labeled peptides.

Because τ_R depends directly on temperature and the solvent viscosity η (which also varies with temperature), it does not reflect solely the intrinsic properties of the tumbling molecule. This motivates the concept of a local tumbling volume

$$V_L = \frac{kT\tau_R}{\eta} \tag{5}$$

Although this is simply a rearrangement of eq 4, V_L reflects the volume of the peptide that is actually reorienting with the nitroxide label assuming that Stokes–Einstein behavior holds at each temperature. The importance of this quantity is that it reflects structural details of the labeled peptide with external environment-dependent quantities removed. However, its interpretation is not necessarily simple, as discussed below.

To this point we have been evaluating data as a function of temperature. Temperature, however, is simply a control parameter that allows for variation in the fractional helicity of the sample. It is also interesting to evaluate V_L directly as a function of fractional helicity obtained from our CD studies, and this is shown in Figure 6 along with the corresponding temperatures along the top axis. The temperature-dependent V_L's for GS-MTSSL are also shown as a reference although this peptide has no CD signal. In this representation, a curve with zero slope indicates ideal SE behavior. Labeled glutathione exhibits a gentle near-linear slope throughout the range studied. Thus, the non-SE behavior shown in Figure 5 can be interpreted as a continuous change in V_L. Phenomenologically we find the temperature dependence of V_L for GS-MTSSL follows $V_L(T) \propto T^{-\alpha}$ where $\alpha \approx 3$. To demonstrate this, we also show the function $V_L(274) \times (274/T)^3$ in Figure 6 (where $V_L(274)$ is the experimental local volume of GS-MTSSL at 274 K), and it clearly overlays the glutathione data. This behavior may be justifiable in terms of idealized polymer theories where polymer persistence lengths are expected to follow inverse power law functions (Doi & Edwards, 1986).

As before, the change for i+4c-MTSSL is quite dramatic. At high fractional helicity the peptide has an SE tumbling volume of 1770 Å^3. We estimate the expected tumbling volume for a hydrated 17-mer helix with standard dimensions (radius ≈ 5 Å, helical pitch = 1.49 Å/residue) and cylindrical shape as 2000 Å, so the observed value is reasonable (as was τ_R). Below Θ = 0.4 fractional helicity, V_L begins a monotonic nonlinear descent and at a fractional helicity of 0.2 V_L has decreased to approximately 55% of the original value. Because the systematic error in our measurements is constant and less than 10% throughout the temperature range, and the random error is approximately ±3%, the observed changes in V_L cannot be explained in terms of experimental error.

Discussion

In this study we have shown that short helical peptides can be substituted with a single Cys and spin-labeled without significant perturbation of the peptide's intrinsic helix-forming tendency. This is fortuitous when one considers that substitutions of nonpolar residues into related peptides can dramatically reduce the helicity (Padmanabhan et al., 1990), although those results appear to be restricted to residues with a branch at the side-chain β carbon. The Cys-MTSSL "residue" was also found to be relatively nonperturbing in bacteriorhodopsin in which there was reduced biological activity in only 3 of 18 spin-labeled mutants (Altenbach et al., 1990). In a similar study, 20 spin-labeled cysteine mutants of colicin E1 showed no reduction of biological activity compared to the native protein (Todd et al., 1989).

Our samples contained nanomole quantities of peptide that were used to gather high-resolution ESR spectra at 5° intervals throughout the thermally controlled α-helix → coil transition. Using rotational correlation times determined from motional-narrowing theory, we observed concomitant changes in the rotational anisotropy and the Stokes–Einstein behavior of the peptide near the midpoint of the transition. We introduced the concept of a local tumbling volume, V_L, which is the apparent volume of peptide that reorients with the nitroxide spin label. The data indicate that V_L decreases with increasing temperature for both GS-MTSSL and i+4c-MTSSL. The way in which V_L decreases is unique for each of the peptides. An examination of V_L vs fractional helicity for i+4c-MTSSL indicates that V_L is the expected value for a rigid 17-mer α-helix at high helicity and decreases only when the helicity drops below 0.4.

A first possible explanation for the non-SE behavior observed for both the labeled GSH and labeled i+4c is that the nitroxide side chain is reorienting relative to the peptide to which it is attached. We believe, however, that this unlikely on the time scale of the rotational correlation times studied here. In order for V_L to reflect peptide geometry, the spin label must be rigidly attached to the peptide on the time scale of the peptide motions studied. If this were not the case, V_L might reflect the reorientation of the spin-labeled side chain relative to the peptide backbone and not the overall tumbling of the peptide–MTSSL complex. However, the results of spin labeling of site-directed cysteine mutants of β-lactamase (unpublished results) and colicin E1 (Todd et al., 1989) indicate that the reorientation of the cysteine–MTSSL side chain on the surface of an α-helix is relatively slow. We found that the spectrum of MTSSL-labeled β-lactamase (MW = 29 500), at room temperature, was well simulated with a model of anisotropic motion and correlation times of 1.3 ns about the unique axis and 6.7 ns about the remaining axes. The longer correlation time is close to that expected for rotational diffusion

of a protein of this size, and the shorter correlation time most likely reflects the motion of the side chain. In accord with this, the published spectra of MTSSL attached to a helical external surface of colicin E1 (MW = 56000) qualitatively appear to indicate even slower motion than for the labeled β-lactamase mutant. Since the measured τ_R for i+4c-MTSSL at room temperature (298 K) is 0.35 ns (Figure 5), motion of the nitroxide with respect to the peptide backbone makes only a minor contribution to τ_R and is unlikely to be responsible for the non-SE behavior exhibited by both labeled peptides.

Our data for i+4c-MTSSL indicate that V_L decreases at fractional helicity below 0.4, and we believe that this indicates the onset of internal flexibility in the peptide. We must now address two issues. First, can the shape of the V_L vs fractional helicity curve be explained in terms of the basic models of the α-helix → coil transition? And second, is V_L at low fractional helicity a reasonable value for a nearly random-coil peptide? We begin by considering both a cooperative model and noncooperative model for the α-helix → coil transition.

V_L from a Cooperative Model of the α-Helix → Coil Transition. The reversible transition from α-helix to random coil, in long polymers, is typically modeled as a highly cooperative process in which nucleation of the first full loop in the helix is an event of low probability ($\sigma \ll 1$ in the language of the Zimm–Bragg model). Upon nucleation, however, it is quite likely that the peptide will zip up to form a complete helix. The consequence of this cooperative model is that an individual peptide will mainly exist in either a completely helical state or a completely random-coil state. States of intermediate helicity are not highly populated. Thus, we can approximate the interconversion process as an equilibrium between coil (C) and helix (H)

$$C \underset{k_2}{\overset{k_1}{\rightleftharpoons}} H \tag{6}$$

with the rate constants k_1 and k_2. The equilibrium constant K and the fractional helicity Θ are then defined as

$$K = \frac{k_1}{k_2} = \frac{\Theta}{1-\Theta} \tag{7}$$

We now develop a line-shape theory based upon a modified Bloch equation approach to incorporate the effects of chemical exchange between the two states of the peptide. We assume that each nitroxide spin label in the sample is attached to a peptide in either an H state or a C state. The only distinction between these states, from the perspective of the label, is the value of the local tumbling volume V_L, and we approximate that the value for $V_{L,H}$ is constant with temperature and $V_{L,C}(T)$ is approximated by $V_{L,C}(274) \times (274/T)^3$ (see Results). Experimentally, we find that the resonance frequencies of the ESR spectral lines do not shift with temperature and this indicates that this exchange process affects only the observed line width $[T_2(M)^{-1}]$. Thus, the observed line shapes are computed from the modified Bloch equation for the Mth line, which is

$$\frac{d}{dt}\begin{pmatrix} M_C^+(M) \\ M_H^+(M) \end{pmatrix} = -\begin{pmatrix} 1/T_{2,C}(M) + k_1 & -k_2 \\ -k_1 & 1/T_{2,H}(M) + k_2 \end{pmatrix}\begin{pmatrix} M_C^+(M) \\ M_H^+(M) \end{pmatrix} \tag{8}$$

where $M_C^+(M)$ and $M_H^+(M)$ refer to the x,y magnetization of the Mth line of the coil and helical states, respectively (Ernst et al., 1987). $T_{2,C}(M)^{-1}$ and $T_{2,H}(M)^{-1}$ refer to the respective line widths and are computed as follows. The τ_R's for a pure helix or coil at each temperature are calculated from T, $\eta(T)$, and $V_{L,H}$ or $V_{L,C}(T)$ with the SE relation in eq 4. Subsequently, the temperature-dependent line widths are calculated from the motional-narrowing theory for nitroxides (which gives rise to eqs 1 and 2) (Goldman et al., 1972).

Each of the hyperfine lines in our experimental spectra are well described by a single Lorentzian line with Gaussian inhomogeneous broadening. This is supported by preliminary spin echo experiments with i+4c-MTSSL, made in the upper end of the temperature regime, where we found that the echo envelope decays monoexponentially (unpublished results). These results indicate that we are in the fast exchange regime where $k_1, k_2 > |T_{2,C}(M)^{-1} - T_{2,H}(M)^{-1}|$. This difference in the T_2's is probably 100 ns or longer, and, therefore, the rate constants used for the simulations are greater than 10^7 s^{-1}. Finally, the rate constants are determined by assuming that k_2 does not vary with temperature and k_1 is varied to reflect Θ from eq 7.

The matrix in eq 8 yields two eigenvalues, and the smaller of these determines the line width for the Mth hyperfine line in the fast exchange regime. (In the intermediate and slow exchange regime a more detailed analysis is required.) The outer two line widths (for $M = +1, -1$) at each temperature are then used to determine B and, hence, a rotational correlation time. From this τ_R, the exchange-averaged V_L is calculated with eq 5. This total process is a rather involved method for the simulation of V_L; however, this approach is useful because it actually simulates the experimental procedure. With this cooperative model there are three adjustable parameters: $V_{L,C}(274)$, $V_{L,H}$, and k_2. In Figure 6 the most successful simulation is shown where $k_2 = 5 \times 10^8$ s^{-1}, $V_{L,H} = 3500$ Å^3, and $V_{L,C}(274) = 800$ Å^3. Beyond $k_2 = 5 \times 10^8$ s^{-1} is the extreme fast exchange limit, and no further change in the V_L vs Θ curve is observed. For $k_2 = 10^{-8}$ s^{-1}, the relationship between V_L and Θ exhibits a positive curvature that does not fit the data at either high or low Θ. (For even smaller values of k_2, the observed line shape is not well described by a single Lorentzian line.) It is apparent from Figure 6 that we were able to fit the low Θ regime; however, we could not find a combination of fitting parameters to duplicate the plateau in the experimental data between Θ = 0.4 and 0.72. Clearly, the exchange theory developed here is based upon several simplifying assumptions; nevertheless, the near agreement in the region of low fractional helicity is suggestive of the underlying dynamic process.

V_L from a Noncooperative Model of the α-Helix → Coil Transition. We now approach the dependence of V_L vs fractional helicity from the perspective of a noncooperative transition in which the sample is approximately homogeneous. In this view, a fractional helicity of 0.3, for instance, indicates that 30% of the amino acids in each peptide are hydrogen bonded in an α-helical configuration. Motivation for such an approach arises from the V_L = constant region, for $\Theta \geq 0.4$, which could not be explained with our cooperative model.

We retain the nucleation behavior, described above in the cooperative model, by assuming that a peptide can have only one contiguous helical segment, and we further assume that $V_L = V_{L,H}$ if the spin label is in a helical segment and $V_L = V_{L,C}(T)$ if the label is in a coil segment. In this view, noncooperativity arises from the coexistence of helical and nonhelical residues within the same peptide, i.e., on average the ends of the helix will be less helical than the central region. In this model, the labeled amino acid in the middle of the peptide must always be in a helical segment when $\Theta > 0.5$. When $\Theta < 0.5$, $P_H(\Theta)$ is determined from the following argument. If M (the total number of residues) is odd and there are k contiguous helical residues, then there will be k con-

figurations that include the central residue within the helical region of the peptide. The total number of configurations with k contiguous helical residues is $M - k + 1$ (Cantor & Schimmel, 1980). If the identity $\Theta = k/M$ and the approximation $M - M\Theta + 1 \approx M(1 - \Theta)$ are used, the probability for finding the central residue in a helical segment is $\Theta/(1 - \Theta)$ as long as $\Theta < 0.5$. If the arguments above are combined, the equilibrium probability of finding the central labeled residue in a helical segment is described by the function

$$P_H(\Theta) = \begin{cases} 1 & \Theta \geq 0.5 \\ \dfrac{\Theta}{(1 - \Theta)} & \Theta < 0.5 \end{cases} \quad (9)$$

The physical implication of this model is the following. When the spin label is in a helical segment, it is attached to a rigid backbone region that reorients with the whole peptide. Conversely, when the spin label is in a coil segment, it is attached to a flexible backbone region that allows for motion of the label with respect to the rest of the peptide.

The dynamics are again described by the reaction given in eq 6 except that now k_1 and k_2 refer to the rates of migration of the helical segment into or away from the spin-labeled region in the middle of the peptide. The equilibrium constant for this process is

$$K = \frac{P_H(\Theta)}{1 - P_H(\Theta)} \quad (10)$$

for which $K = \infty$ when $\Theta > 0.5$. Again we use eq 8 in the same way as discussed above with $k_1 = Kk_2$ (and K from eqs 9 and 10). In Figure 6 the most successful simulation is shown for this model where $k_2 = 10^7\ s^{-1}$, $V_{L,H} = 1800\ Å^3$, and $V_{L,C}(274) = 1600\ Å^3$. As above, larger k_2 does not change the curve in an appreciable way. Smaller k_2 gives a sigmoidal relationship between V_L and Θ. The agreement between theory and experiment for this model is reasonable. The noncooperative model predicts a kink near $\Theta = 0.5$, and this is not found in the experimental data; however, all other regions of the curve are fairly consistent.

Which Model Is Preferred? Examination of Figure 6 reveals that the cooperative two-state model fits the data for low Θ, whereas the noncooperative approach almost fits over the entire range of Θ. On this basis, we might conclude that the noncooperative model is preferable. However, the vast majority of research into the α-helix → coil transition indicates that the transition is highly cooperative for long polymers and moderately cooperative for shorter peptides such as the i+4. Therefore, we must treat such a conclusion with skepticism. The models developed above include several simplifying assumptions including the temperature independence of $V_{L,H}$. We could relax this particular assumption and develop models with a temperature-dependent $V_{L,H}$ to fit the data more accurately. It is difficult, however, to extract meaningful results from models with a large number of fitting parameters.

Nevertheless, if the transition is somewhat cooperative, the inconsistency between the model and the data at high fractional helicity suggests that there is a persistency of the rigid helical state beyond that seen in the CD data. We propose that this persistency may arise from the salt bridges formed by the $Glu^-\cdots Lys^+$ side chains. As the fractional helicity decreases from the maximum value of approximately 0.72, the dihedral angles required for a CD-observable α-helix begin to distort. Nevertheless, the peptide as a whole maintains a high degree of structural rigidity, and this rigidity begins to break down only when the fractional helicity drops below 0.4. The implication of this is that the salt bridges influence the structure only when Θ is high. If this hypothesis is correct, then short helical peptides without salt bridges will follow the predictions of our cooperative exchange model. We further suggest that ESR experiments performed on end-labeled analogues of the i+4 peptide will allow us to conclusively distinguish between the cooperative and noncooperative models for α-helix formation.

The Magnitude of V_L at Low Fractional Helicity. The experimental data in our studies indicate that V_L decreases with decreasing Θ. We believe this indicates the onset of segmental motion in the peptide. In early theoretical studies of the α-helix → coil transition, Miller and Flory (1966) showed that short helical homopolymers of alanine ($N < 35$) exhibit an increase in the average end-to-end distance as the fractional helicity decreases. Their calculation reflects the compact structure of short α-helices vs the more loose structure of random coils. If the backbone of the random-coil peptide were rigid, on the time scale of our experiments, then we might actually expect an increase in V_L with decreasing Θ.

More insight into this problem is obtained from recent theoretical studies on the segmental motion of polypeptides. Several systems were studied, including a 50-mer of polyalanine, by using a Rouse–Zimm model of polymer dynamics (Perico, 1989). The calculations indicated that even residues near the middle of the peptide have a high degree of internal flexibility. The persistence length was on the order of seven residue lengths, meaning that reorientation more closely followed the local hydrodynamics of a short peptide than a 50-mer. Our results are qualitatively consistent with with these theoretical results. Thus, at high fractional helicity, the i+4c-MTSSL tumbles as a rigid hydrogen-bonded peptide, and the nitroxide reflects the overall tumbling motion. At very low Θ, the behavior is more random-coil-like, and the nitroxide reflects the segmental motion of the backbone in accordance with the theoretical calculations.

Conclusion

We have shown that helical peptides can be Cys-substituted and spin-labeled in a site-specific fashion with minimal perturbation to the peptide's secondary structure. Correlation times extracted from the ESR spectra indicate that the attachment is rigid on the subnanosecond time scale. Using the concept of a local tumbling volume, we showed that the backbone of this salt-bridged i+4 helix becomes flexible only when the fractional helicity is below 40%. We further showed that a simple cooperative model is not sufficient to explain the behavior of V_L vs Θ.

NMR has recently become a powerful tool for studying the structure and dynamics of proteins. Lately it has also been applied to helical peptides (Osterhout et al., 1989). Under the appropriate conditions, NMR can reveal fine geometric and dynamic details. ESR, however, offers several advantages, which makes the two approaches complementary. First, ESR experiments can be performed with microgram quantities of peptide, whereas NMR usually requires several milligrams for high-resolution work. Thus, ESR studies can be performed on specialized peptides without large scale preparations. Second, ESR spectra are gathered in several minutes so that the behavior of a peptide can be studied over a range of temperatures and conditions. For a quantitative analysis of the α-helix → coil transition, one must have data throughout the transition temperature range. Third, ESR spectra are readily analyzed in terms of nanosecond motions. NMR experiments can also reveal nanosecond motions (Mirau & Bovey, 1986); however, more spectral analysis is required. Finally, peptides of the type studied here are constructed from only two or three

different amino acid types. We anticipate that the NMR spectra of such systems will yield many overlapping lines and would be somewhat difficult to interpret. Thus, both NMR and ESR experiments require a labeling approach for site-specific information. The use of labels is ubiquitous throughout spectroscopy, and the success of such experiments requires that independent tests be performed to examine the extent of the label's perturbation of the system. In this work we have used CD to quantitatively determine that this perturbation is small.

The methodology developed and applied in our work can now be used to probe a range of exciting problems. For instance, examination of the behavior of a helical peptide labeled near the end will give further insight into the degree of cooperativity in the α-helix → coil transition. Addressing another point, it is known that replacing alanine with other residues (i.e., valine) can lower the fractional helicity (Padmanabhan, 1990). From CD studies it is not clear whether this is a local or global effect. Our approach may resolve such points. Finally, we believe that our methods can be applied to larger peptide systems, such as helix bundles, to identify nucleation sites in the folding process.

Acknowledgments

The i+4c peptide was a generous gift from Dr. Susan Marqusee and Dr. Robert Baldwin and we are grateful for their support and helpful discussions. We thank Mr. John Williams and Mr. Wayne Fiori for the calculation of the peptide structure in Figure 1. Mr. Walter Escobar and Dr. Anthony Fink kindly provided the site-directed mutant of β-lactamase (Glu_{166} → Cys) as part of an ongoing collaboration. Mass spectra were provided by the Mass Spectrometry Facility, University of California, San Francisco, supported by NIH Division of Research Resources Grants RR01614 and RR04112.

Registry No. it4c, 133495-37-1; it4c-MTSSL, 133495-38-2; GS-MTSSL, 133522-72-2.

References

Altenbach, C., Marti, T., Khorana, G. H., & Hubbell, W. L. (1990) *Science 248*, 1088–1092.

Bales, B. L. (1989) in *Biological Magnetic Resonance* (Berliner & Reuben, Eds.) Chapter 2, Plenum, New York.

Beth, A. H., & Robinson, B. H. (1989) in *Biological Magnetic Resonance* (Berliner & Reuben, Eds.) Chapter 4, Plenum, New York.

Brown, J. E., & Klee, W. A. (1971) *Biochemistry 10*, 470–476.

Cantor, C. R., & Schimmel, P. R. (1980) *Biophysical Chemistry*, Freeman, San Francisco, CA.

Capiomont, A., Chion, B., Lajzerowicz-Bonneteau, J., & Lemaire, H. (1974) *J. Chem. Phys. 60*, 2530–2535.

Doi, M., & Edwards, S. F. (1986) *The Theory of Polymer Dynamics*, Clarendon, Oxford.

Ernst, R. R., Bodenhausen, G., & Wokaun, A. (1987) *Principles of Nuclear Magnetic Resonance in One and Two Dimensions*, Clarendon, Oxford.

Goldman, S. A., Bruno, G. V., Polnaszek, C. F., & Freed, J. H. (1972) *J. Chem. Phys. 56*, 716–735.

Hwang, J. S., Mason, R. P., Hwang, L., & Freed, J. H. (1975) *J. Phys. Chem. 79*, 489–511.

Hyde, J. S., & Subczynski, W. K. (1984) *J. Magn. Reson. 56*, 125–130.

Marqusee, S., & Baldwin, R. L. (1987) *Proc. Natl. Acad. Sci. U.S.A. 84*, 8898–8902.

Marqusee, S., Robbins, V. H., & Baldwin, R. L. (1989) *Proc. Natl. Acad. Sci. U.S.A. 86*, 5286–5290.

Marsh, D. (1989) in *Biological Magnetic Resonance* (Berliner & Reuben, Eds.) Chapter 5, Plenum, New York.

Miller, W. G., & Flory, P. J. (1966) *J. Mol. Biol. 15*, 298–314.

Mirau, P. A., & Bovey, F. A. (1986) *J. Am. Chem. Soc. 108*, 5130–5134.

Nelson, J. W., & Kallenbach, N. R. (1986) *Proteins 1*, 211–217.

Noji, S., Nomura, T., & Yamaoka, K. (1980) *Macromolecules 13*, 1114–1120.

Osterhout, J. J., Baldwin, R. L., York, E. J., Stewart, J. M., Dyson, H. J., & Wright, P. E. (1989) *Biochemistry 28*, 7059–7064.

Padmanabhan, S., Marqusee, S., Ridgeway, T., Laue, T. M., & Baldwin, R. L. (1990) *Nature 344*, 268–270.

Perico, A. (1989) *Biopolymers 28*, 1527–1540.

Shoemaker, K. R., Kim, P. S., Brems, D. N., Marqusee, S., York, E. J., Chaiken, I. M., Stewart, J. M., & Baldwin, R. L. (1985) *Proc. Natl. Acad. Sci. U.S.A. 82*, 2349–2353.

Stone, T. J., Buckman, T., Nordio, P. L., & McConnell, H. M. (1965) *Proc. Natl. Acad. Sci. U.S.A. 54*, 1010–1017.

Todd, A. P., Cong, J., Levinthal, F., Levinthal, C., & Hubbell, W. L. (1989) *Proteins 6*, 294–305.

Tsutumi, A., Perly, B., Forchioni, A., & Chachaty, C. (1978) *Macromolecules 11*, 977–986.

Weast, R. C. (1973) *Handbook of Chemistry and Physics*, 54th ed., CRC Press, Cleveland, OH.

Windle, J. J. (1981) *J. Magn. Reson. 45*, 432–439.

Zager, S. A., & Freed, J. H. (1982) *J. Chem. Phys. 77*, 3344–3359.

Zimm, B. H., & Bragg, J. K. (1959) *J. Chem. Phys. 31*, 526–535.